# Strong CH+ J = 1–0 emission and absorption in DR21*

*Astronomy & Astrophysics* manuscript no. 14671
July 9, 2010




LETTER TO THE EDITOR

# Strong $CH^+$ $J$=1–0 emission and absorption in DR21 ⋆

E. Falgarone[1], V. Ossenkopf[2,3], M. Gerin[1], P. Lesaffre[1], B. Godard[4], J. Pearson[5], S. Cabrit[6], Ch. Joblin[7], A. O. Benz[8], F. Boulanger[4], A. Fuente[9], R. Güsten[10], A. Harris[11], T. Klein[10], C. Kramer[12], S. Lord[13], P. Martin[14], J. Martin-Pintado[15], D. Neufeld[16], T. G. Phillips[17], M. Röllig[2], R. Simon[2], J. Stutzki[2], F. van der Tak[3,18], D. Teyssier[19], H. Yorke[5], N. Erickson[20], M. Fich[21], W. Jellema[3], A. Marston[19], C. Risacher[3], M. Salez[6], F. Schmülling[2]

*(Affiliations can be found after the references)*

Received / Accepted

**ABSTRACT**

We report the first detection of the ground-state rotational transition of the methylidyne cation $CH^+$ towards the massive star-forming region DR 21 with the HIFI instrument onboard the *Herschel* satellite. The line profile exhibits a broad emission line, in addition to two deep and broad absorption features associated with the DR 21 molecular ridge and foreground gas. These observations allow us to determine a $^{12}CH^+$ $J$=1–0 line frequency of $\nu$=835137±3 MHz, in good agreement with a recent experimental determination. We estimate the $CH^+$ column density to be a few $10^{13}$ cm$^{-2}$ in the gas seen in emission, and $> 10^{14}$ cm$^{-2}$ in the components responsible for the absorption, which is indicative of a high line of sight average abundance $[CH^+]/[H] > 1.2 \times 10^{-8}$. We show that the $CH^+$ column densities agree well with the predictions of state-of-the-art C-shock models in dense UV-illuminated gas for the emission line, and with those of turbulent dissipation models in diffuse gas for the absorption lines.

**Key words.** Astrochemistry - ISM : molecules - ISM : kinematics and dynamics - Turbulence

## 1. Introduction

The methylidyne ion $CH^+$ was among the first molecules to be detected in the interstellar medium (ISM) Douglas & Herzberg (1941). This reactive ion is prevalent in the diffuse ISM with column densities several orders of magnitude above the predictions of UV-driven equilibrium models (see references in Godard et al. 2009). Apart from the strong emission lines of $CH^+$ detected in both the envelope of the Red Rectangle Hobbs et al. (2004) and NGC 7027 Cernicharo et al. (1997), all other observations are absorption lines detected at visible wavelengths in the spectra of nearby stars. $CH^+$ is a light molecule and its rotational lines lie at submillimeter and far infrared wavelengths. The exact frequencies of the rotational transitions of $CH^+$ have remained elusive for a long time because of the extreme reactivity of $CH^+$ and the difficulty in isolating it in the laboratory Pearson & Drouin (2006). Recent laboratory measurements have led to $\nu$ = 835.137498(20) GHz for the ground-state transition (Amano, 2010). Ground-based astronomical detection of $^{12}CH^+$(1-0) is prevented by its proximity to a strong atmospheric line of water vapor. The ground-state frequency of the isotopologue $^{13}CH^+$, redshifted by ∼ 5 GHz, has superior sky transmission. It has been detected at the Caltech Submillimeter Observatory towards several massive star-forming regions of the inner Galaxy (Falgarone et al. in prep., Falgarone et al. 2005). The $^{12}CH^+$ abundances averaged along these long lines-of-sight (*los*), confirm the high abundances of this species inferred from visible observations in the local ISM, $[CH^+]/[H] \sim 8\times10^{-9}$ on average. In this paper, we report the detection of the $^{12}CH^+$ $J$=1–0 transition towards the massive star-forming region DR21, presented in Sect. 2. The HIFI observations are described in Sect. 3. The results, given in Sect. 4, are compared to models in Sect. 5.

## 2. The DR 21 region

The massive star-forming region DR 21 is located in the Cygnus X complex at an average distance of 1.7 kpc, that of the Cyg OB2 stellar association (see reviews by Jakob et al. 2007; Schneider et al. 2010). The DR 21 molecular core is one of the most massive cores in the Galaxy ($2.5\times10^4$ $M_\odot$ at the 1 pc-scale) (Kirby 2009). It is located in front of the main DR 21 HII region comprising five compact HII regions and more diffuse ionised gas (Roelfsema et al. 1989; Wilson et al. 1995; Cyganowski et al. 2003).

The star-forming region DR 21 itself is known to host one of the most powerful molecular outflows shining in vibrationally excited $H_2$ (e.g., Garden & Carlstrom 1992). The outflow source is heavily extinguished by more than 100 magnitudes, and its location is not accurately known (Wilson et al. 1995). High velocity HI (up to 90 kms$^{-1}$) associated with the molecular outflow has been detected by the VLA (Russell et al. 1992), indicating that the molecular outflow may be driven by this atomic jet. The outflow shows up as broad wings in CO and $HCO^+$ lines Kirby (2009). At the position of the HIFI beam, the $v = 1 - 0$ S(1) $H_2$ emission line has a similar broad width Nadeau & Béland (1988); Cruz-Gonzalez et al. (2007) to that of the SiO emission (Motte et al. 2007).

Some line profiles imply that there is foreground gas, which is probably associated with the Cygnus X complex Jakob et al. (2007); Schneider et al. (2010). A foreground component associated with W75N shows up as weak emission lines at $v_{LSR}$ ∼ 8 km s$^{-1}$ in low excitation transitions of CO and $HCO^+$ or atomic carbon, and in the atomic oxygen fine-structure line, with $N(O) > 5 \times 10^{18}$ cm$^{-2}$ Poglitsch et al. (1996). The total hydro-

⋆ *Herschel* is an ESA space observatory with science instruments provided by European-led Principal Investigator consortia and with important participation from NASA.

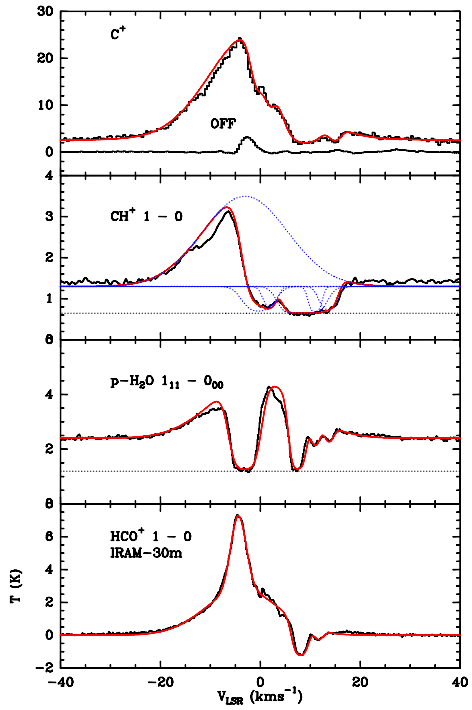


**Fig. 1.** [CII], $CH^+$(1-0) and p-$H_2O$ *Herschel*/HIFI spectra (top panels) and $HCO^+$(1-0) IRAM-30m spectrum (bottom panel) (Schneider et al. 2010). The HIFI spectra are taken in DSB, hence saturated lines reach to half the continuum level (dotted lines). The weak line in the $C^+$ panel is that of an intermediate OFF position. The $CH^+$ (J=1-0) spectrum is shown assuming a rest frequency of 835137 MHz. The Gaussian velocity components involved in the empirical model of the $CH^+$ profile are shown (dotted blue curves) as well as the resulting models for all lines (red curves) (see Sect. 4).

gen column density of this foreground material is estimated to be $N(\mathrm{H}) \sim 1.4 \times 10^{22}$ cm$^{-2}$ for an elemental abundance ratio [O]/[H] =3.45 $\times 10^{-4}$ Oliveira et al (2005), in coherence with $N(\mathrm{H}) = (1.3 \pm 0.4) \times 10^{22}$ cm$^{-2}$ inferred from K extinction to DR21 (Marshall et al. 2006). This component is also detected in atomic hydrogen, which indicates that there is saturated absorption of between -5 and 18 km s$^{-1}$ Roberts et al. (1997). Its estimated HI column density, if $T_s = 20K$, is $N(\mathrm{HI}) > 1.5 \times 10^{21}$ cm$^{-2}$.

## 3. HIFI observations

All FIR spectra presented here were obtained in the course of performance verification observations with the HIFI instrument (Pilbratt et al. 2010; de Graauw et al. 2010). Since their main goal was to demonstrate the functionality and performance of the different observing modes, the spectra were taken with a large variety of observing strategies. Most observations were only single-point observations towards the central position of the DR21 HII region at RA=20h39m01.1s, Dec=42°19′43.0″ (J2000). At the frequencies around 1 THz discussed here, the *Herschel* beam covers about 20″ HPBW (or 0.16 pc at 1.7 kpc). Here, we only present data from the wideband spectrometer (WBS) that provides a resolution of 1.1 MHz, corresponding to 0.2 km/s (at 1900 GHz) and 0.4 km/s (at 835 GHz).

The $CH^+$ spectrum at 835 GHz was obtained in a single-point load-chop observing mode without OFF reference. It uses

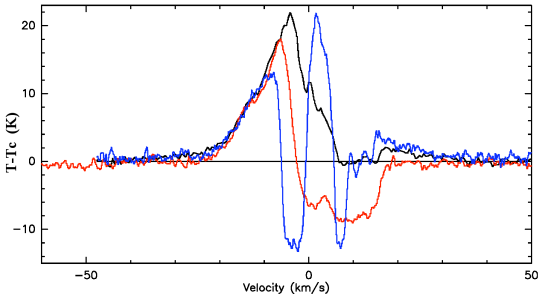


**Fig. 2.** Superimposition of the $CH^+$ (red), $C^+$ (black), and p-$H_2O$ (blue) spectra (from which the continuum has been subtracted) to illustrate the good coincidence of the blue wing of the line profile when the $CH^+$(1-0) frequency is $\nu$ = 835.137 GHz. We note also the coincidence of the absorption features in $CH^+$(1-0) and $C^+$.

the internal cold load as reference, having the advantage that we can exclude any self-chopping effects in the line profiles. The mode has, however, the disadvantage that the different optical paths towards the sky and the internal calibration load sometimes lead to standing wave differences that are detected as baseline ripples. We subtracted these manually using the HifiFitFringe pipeline tool. The total integration time on the source was 48 s leading to a noise level of 0.1 K for the combination of the spectra from both polarisations at the WBS resolution.

The $H_2O$ $1_{11}-0_{00}$ (1113 GHz) line was observed in the frame of a spectral scan in a load-chop mode and an on-source integration time of 30 s. The baseline was calibrated on a distant OFF position (20h37m10s, 42°37′00″) because the first selected OFF position, closer to the ON, retained some signal (see Fig. 1). The [CII] line was detected in one of the first double-beam switch raster mapping observations in which neither the logic of the mapping mode worked as expected nor the pointing of the instrument was yet known. The instrument pointing was measured afterwards and the map coordinates were corrected by hand to include the correct offsets. A comparison of the integrated [CII] intensities in the shifted map with the MSX 8 $\mu$m band shows a very good agreement, confirming the accuracy of the correction. The observations were taken on a 7″ raster that included a 14 s on-source integration time at each point. To obtain a spatial resolution comparable to that of the other two lines, the map was convolved with a Gaussian beam of 20″ at the DR 21 central position.

## 4. Results of the line profile analysis

The HIFI spectra are displayed in Fig. 1 with, for comparison, an IRAM-30m spectrum of $HCO^+$(1-0) (Schneider et al. 2010). The line profiles exhibit both complex emission and absorption because of the multiplicity of velocity components and gas physical conditions within the beam. The line integrated areas in emission and absorption are remarkably comparable. This would lead to a weak or non-detection with low spectral resolution instruments. The dashed lines in the $CH^+$ and p-$H_2O$ spectra, at about half the continuum level, reveal the broad velocity ranges across which the absorption lines are saturated.

The $CH^+$(1-0), $C^+$ and p-$H_2O$ spectra, plotted after their continuum has been subtracted, are superimposed in Fig. 2 for the frequency of the $CH^+$ $J$=1–0 line set to 835.137 GHz. We propose in Sect. 5 that the broad line emission originates from a shock associated with the outflow, and we show that the three species, $CH^+$, $C^+$ , and $H_2O$ are connected with each other in the

**Table 1.** Empirical models of the broad emission profiles

| Line | $v$ | $\Delta v$ | $T$ |
|---|---|---|---|
| | km s$^{-1}$ | km s$^{-1}$ | K |
| $CH^+$ | -3.0 | 20.0 | 2.2 |
| p-$H_2O$ | -1.0 | 20.0 | 2.16 |
| $C^+$ | -1.8 | 20.0 | 22 |
| | 0 | 80.0 | 1.0 |
| $HCO^+$ | -3.6 | 17.0 | 2.8 |

shock chemistry. The good agreement (within $\pm$ 1 km s$^{-1}$) between the blue wing of the emission line profiles of these three species allows us to adopt $\nu$ = 835137 $\pm$ 3 MHz as the rest frequency of the $^{12}CH^+$(1-0) line, which is remarkably consistent with the experimental value measured by Amano (2010).

The $CH^+$ $J$=1–0 line profile can be decomposed into a broad emission line and a series of absorption features. We used information from the line profiles of CO and $HCO^+$ $J$=1–0 (see Fig. 1), the spectra of atomic carbon Jakob et al. (2007), and other HIFI spectra (Ossenkopf et al. 2010; van der Tak et al. 2010) to constrain the velocity and linewidth of these components. Since the $^{13}CH^+$ line has not been observed, the actual $CH^+$ emission profile is unknown. We had to rely on the symmetric shapes of the CO emission lines to model the broad emission wings with Gaussians adjusted on the blue wings of the lines (Table 1). Over the velocity range -5 to 17 km s$^{-1}$, not only the continuum level but also the core line emission is absorbed by intervening gas. The broad emission lines ($\Delta v$ = 20 km s$^{-1}$, see Table 1) correspond to the emission associated with the outflow shock (see Sect. 5). A still broader component in the [CII] line has a width similar to that of the H66$\alpha$ recombination lines Roelfsema et al. (1989). Self-absorption features in the range $\sim -3$ to 2 km s$^{-1}$, caused by the close environment of the DR21 core, are visible in CO, $HCO^+$(4-3), and other dense gas tracers (e.g., $NH_3$ inversion lines). The absorption dip at this velocity is more prominent in the $H_2O(1_{1,1} - 0_{0,0})$ profile as expected from the high critical density of this transition. We disregarded this velocity range in our analysis because of the unknown line intensity of the dense core emission. In contrast, the absorption at $v > 7$ km s$^{-1}$ corresponds to the gas that is most likely to be associated with the W75N cloud in the Cygnus X complex. Its velocity coverage is very similar in the $CH^+$ and $C^+$ spectra. We fitted three components in this velocity range, guided by the absorption features of the $HCO^+$ $J$=1–0 and $H_2O$ profiles at $v_{LSR}$ = 7.5, 11, and 13.7 km s$^{-1}$shown in Fig. 1, the resulting profiles being in red.

The $CH^+$ column density of the emission line was determined by assuming that it is optically thin. This is consistent with the $^{13}CH^+$(1-0) line not being detected in emission towards galactic massive star-forming regions (Falgarone et al. in prep., Falgarone et al. 2005). The total $CH^+$ column density was therefore assumed to scale with the line integrated area (in K km s$^{-1}$) with a coefficient that depends on the excitation temperature. For 40 K< $T_{ex}$ < 100 K, the range of $T_{ex}$ that minimizes $N(CH^+)$, a lower limit $N_{em}(CH^+) = 7 \times 10^{11}$ cm$^{-2}$ $\int T(v)dv$ was obtained, using the spontaneous decay rate $A_{10} = 5.9 \times 10^{-3}$ s$^{-1}$ inferred from the dipole moment, $\mu$ = 1.62 D Kobayashi et al. (1993). In absorption, we inferred the column density from the integral of the optical depth (in km s$^{-1}$) to be $N_{abs}(CH^+) = 3.3 \times 10^{12}$ cm$^{-2}$ $\int \tau(v)dv$. It is almost independent of $T_{ex}$ as long as $T_{ex} << h\nu/k$ = 39K, an approximation that is valid for gas of density much lower than the critical density of the transition (> $10^6$ cm$^{-3}$) and not closely associated with intense FIR radiation. The resulting $CH^+$ column densities are given in Table 2.

**Table 2.** $CH^+$ Column densities

| Component | $T_{ex}$ | $N(CH^+)$ |
|---|---|---|
| | K | cm$^{-2}$ |
| Broad line emission | 40K < $T_{ex}$ < 100K | $2.2 \times 10^{13}$ |
| Foreground absorption | 3.0 | > $1.7 \times 10^{14}$ |

Those of the saturated absorption components are lower limits. Although the Gaussian decomposition is by no means unique, it provides an estimate of both the detected column densities and the $CH^+$ abundance relative to the total hydrogen $[CH^+]/[H] > 1.2 \times 10^{-8}$ in the diffuse gas. We note that the [CII] line opacity of the foreground gas, averaged over 10 km s$^{-1}$, is $\tau_{[CII]} > 1.8$. This opacity limit corresponds to a $C^+$ column density larger than $2 \times 10^{18}$ cm$^{-2}$ for gas of density lower than the critical density of the transition $n_{cr}(C^+)$, i.e. $\sim$ a few $10^3$ cm$^{-3}$, whatever the line excitation temperature (Crawford et al. 1985). The required $C^+$ column density is much larger if the transition is thermalized, i.e. $n >> n_{cr}(C^+)$. From the estimated gas column of $1.4 \times 10^{22}$ cm$^{-2}$, the expected $C^+$ column is $\sim 2 \times 10^{18}$ cm$^{-2}$, assuming a gas-phase carbon abundance of $1.4 \times 10^{-4}$. This value is in close agreement with that derived for the low density limit, strengthening the association of the foreground absorption with gas of densities lower than $\sim$ a few $10^3$ cm$^{-3}$.

## 5. Comparison with model predictions

The only formation route of the molecular ion $CH^+$ is understood to be initiated by the reaction $C^+ + H_2 \rightarrow CH^+ + H$, which is highly endoenergic ($\Delta E/k$ =4640 K). The formation of $CH^+$ in the cold interstellar medium therefore requires suprathermal energy. Several scenarios have been investigated : C-shocks (Pineau des Forêts et al. 1986 (@), highly illuminated and dense photon-dominated regions (PDR) where $C^+$ reacts with vibrationally excited $H_2$ (Sternberg & Dalgarno 1995; Agundez et al. 2010), turbulent interfaces between the warm and cold neutral medium (Lesaffre et al. 2007), and regions of intermittent turbulent dissipation (TDR models, Godard et al. 2009). In the first and last models, ion-neutral friction plays a major role.

For the DR 21 core, it is unclear which processes are at work in the $CH^+$ formation. Broad ($\Delta v$ = 20 km s$^{-1}$) emission lines of SiO Motte et al. (2007) and vibrationally excited $H_2$ Cruz-Gonzalez et al. (2007), similar to the broad emission in the HIFI profiles, are observed and suggest the influence of a shock. We now present a preliminary attempt to account for the observed column densities of $CH^+$ in this highly irradiated environment.

### 5.1. $CH^+$ emission line: C-shock models

We used a steady-state model for C-shocks with time-dependent chemistry and ionization (Flower & Pineau des Forêts 2003). The chemical network was supplemented with the relevant photo-reactions (Pineau des Forêts, priv. comm.). The $H_2$ and CO self-shielding were assumed to be those of a PDR model at $n_H = 10^4$ cm$^{-3}$. We adopted a pre-shock density $n_H = 10^4$ cm$^{-3}$, a shock velocity $v_s$=20 km s$^{-1}$, a magnetic field $B$ = 200$\mu$G (from the measure of magnetic field in Roberts et al. 1997), and a standard cosmic-ray ionisation rate of $\zeta = 5 \times 10^{-17}$s$^{-1}$. We stopped the computation of the shocks at a neutral flow time of $10^4$ yr, which corresponds to the estimated dynamical age of the outflow (lobes of 0.5 pc for a jet velocity up to 100 km s$^{-1}$). The $CH^+$ column-density was found to have already reached a

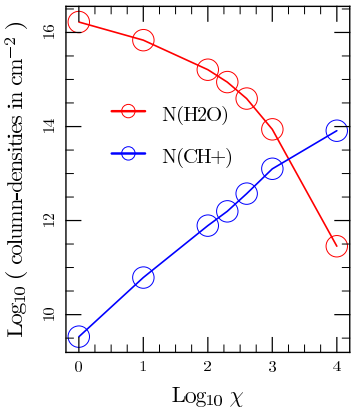


**Fig. 3.** $CH^+$ (blue) and $H_2O$ (red) column densities integrated through the C-shock model (see text) for a broad range of UV-field irradiations $\chi$. The shielding of the shocked material is $A_v$ = 1. We note the opposite behaviours of $CH^+$ and $H_2O$ with $\chi$.

plateau at this stage in the shock, so the $CH^+$ results are insensitive to that choice of age.

Although the incident radiation field is estimated to be $\chi = 10^5$ in ISRF units Ossenkopf et al. (2010) for the material closest to the HII region, we keep this value as a free parameter. Figure 3 displays the total column densities of $CH^+$ and $H_2O$ as a function of the adopted external radiation field. Its effect turns out to be quite interesting: a strong radiation field ($\chi > 10^3$) is needed to account for the large observed $CH^+$ column density. It is the enhanced photo-dissociation of $CH_2^+$ and $CH_3^+$, both products of the rapid hydrogenation of $CH^+$ in the shock, that increases the abundance of $CH^+$ as $\chi$ increases. The shock model also predicts that both $CH^+$ and $H_2O$ are rather well distributed across the various velocity slices of the shock. This supports the assumption that the $CH^+$ and $H_2O$ blue line wings are similar, underlying the $CH^+$ line frequency determination.

### 5.2. $CH^+$ absorption lines: turbulent dissipation models

The large $CH^+$ column density observed in the foreground component corresponds to a *los* average of the $CH^+$ abundance, $[CH^+]/[H]_{ave} > 1.2 \times 10^{-8}$, for $N(H) = 1.4 \times 10^{22}$ cm$^{-2}$ (see Sect. 2). It can be reproduced in the framework of TDR models. At any time, a very large number of tiny regions ($l \sim 100$ AU), altogether filling a small fraction of the entire *los*, are developing a transient warm chemistry triggered by dissipation bursts where local $CH^+$ abundances reach $10^{-6}$ (Godard et al. 2009). The filling factor of the ensemble of these tiny structures is set by the energy transfer rate in the turbulent cascade, $\epsilon = \rho v_l^3/l$, identified with the turbulent dissipation rate. The resulting average abundance is found to scale as $[CH^+]/[H]_{ave}=6.4\times10^{-9}(\epsilon/\epsilon_0)(n_H/50\,\mathrm{cm}^{-3})^{-2.6}$ for an ambient radiation field $\chi = 3$ in ISRF units, where $n_H$ is the density of the gas in which the bursts occur and $\epsilon$ is a non-local quantity of galactic average $\epsilon_0 = 2\times10^{-25}$ erg cm$^{-3}$s$^{-1}$ (see Godard et al. 2009). Fluctuations by two orders of magnitude are observed in the ISM about that galactic average, the highest values being reached in active star-forming regions, such as Cygnus X. We thus expect $\epsilon$ to be up to 100 times higher than average in Cygnus X, so that the observed $CH^+$ abundance can be produced by intermittent dissipation of turbulence occurring in gas of density up to $\sim 250$ cm$^{-3}$. The total number of tiny structures along that 1.7 kpc *los* is found to scale as $\sim 3.5\times10^3(\epsilon/\epsilon_0)(n_H/50\,\mathrm{cm}^{-3})^{-2}$.

## 6. Conclusion

We have detected the line profile of $CH^+$(1-0) towards the DR 21 massive star-forming region with the HIFI instrument, obtaining several major results. The line is a combination of broad emission and almost saturated broad absorption, which have comparable integrated areas. The rest-frame frequency of the $CH^+$ $J$=1–0 line is inferred to be $\nu = 835137 \pm 3$ MHz. For the gas seen in emission, the $CH^+$ column density, of about $10^{13}$ cm$^{-2}$, compares well to predictions of C-shock models propagating in dense, highly illuminated gas. Additional chemical modelling (and radiative transfer calculations) are needed to confirm the C-shock framework and exploit the other line signatures. The large $CH^+$ column density in the foreground gas, $N(CH^+) \sim 10^{14}$ cm$^{-2}$, can be explained by the turbulent dissipation models in diffuse gas and confirms the large opacity of that line in the diffuse molecular gas,

*Acknowledgements.* HIFI has been designed and built by a consortium of institutes and university departments from across Europe, Canada and the United States (NASA) under the leadership of SRON, Netherlands Institute for Space Research, Groningen, The Netherlands, and with major contributions from Germany, France and the US. Consortium members are : Canada: CSA, U. Waterloo; France : CESR, LAB, LERMA, IRAM; Germany : KOSMA, MPIfR, MPS; Ireland : NUI Maynooth; Italy : ASI, IFSI-INAF, Osservatorio Astrofisico di Arcetri-INAF; Netherlands : SRON, TUD; Poland : CAMK, CBK; Spain : Observatorio Astronòmico Nacional (IGN), Centro de Astrobiologia; Sweden : Chalmers University of Technology - MC2, RSS & GARD, Onsala Space Observatory, Swedish National Space Board, Stockholm University - Stockholm Observatory; Switzerland : ETH Zurich, FHNW; USA : CalTech, JPL, NHSC. MG and EF acknowledge the support from the Centre National de Recherche Spatiale (CNES). Part of this work was supported by the German *DeutscheForschungsgemeinschaft, DFG* project # Os177/1–1. We thank G. Pineau des Forêts for providing us with his version of the code for C-shock models.

## References

Agundez M., Goicoechea J.R., Cernicharo J. et al. 2010 ApJ 713, 662
Amano, T. 2010 ApJ accepted
Cernicharo J. et al. 1997 ApJL 483 L65
Crawford, M.K., Genzel, R., Townes C.H. et al. 1985 ApJ 291, 755
Cruz-Gonzalez I., Salas L., Hiriart D. 2007 Rev Mex. A. & A. 43, 337
Cyganowski C.J., Reid M.J., Fish V.L. & Ho P.T.P. 2003, ApJ 596, 344.
Davis C.J., Kumar M.S.N., Sandel G. et al. 2007 MNRAS 374 29
Douglas, A.E., Herzberg,G, 1941 ApJ 94 381.
Falgarone E., Phillips T.G., Pearson J.C., 2005, ApJ 634, L149.
Flower D. R., Pineau des Forêts G., 1998, MNRAS, 297, 1182
Flower D. R., Pineau des Forêts G., 2003, MNRAS, 343, 390
Garden R.P., Carlstrom J.E., 1992, ApJ 392, 602.
Godard B., Falgarone E., Pineau des Forêts G. 2009 A&A 495 847
de Graauw T. et al. 2010, this volume
Hobbs, L.M., et al. 2004 ApJ 615, 947
Jakob H., Kramer C., Simon R., et al. 2007, A&A 461, 999.
Kirby L., 2009, ApJ 694, 1056.
Kobayashi R., Koch H. & Meyer D.N. 1993 Chem. Phys. Lett. 211 94
Lesaffre P., Gerin M., Hennebelle P., 2007, A&A, 469, 949
Marshall D.J., Robin A.C., Reylé C., et al. 2006 A&A 453, 635
Motte, F., Bontemps, S., Schilke, P. et al. 2007 A&A 476, 1243
Nadeau D., Béland S., 1988, AJ 95, 136.
Oliveira C.M., Dupuis J., Chayer P., Moos H.W., 2005, ApJ 625, 232.
Ossenkopf, V., Röllig, M., Simon, R., Schneider, N. et al. 2010, this volume
Pearson J.C. & Drouin B.J. 2006 ApJ 647, L83
Pilbratt G. et al. 2010, this volume
Pineau des Forêts G. et al., 1986, MNRAS, 220, 801
Poglitsch A., Herrmann F., Genzel R., et al., 1996, ApJ 462, L43.
Roberts D.A., Dickel H.R., Goss W.M., 1997, ApJ 476, 209.
Roelfsema P.R., Goss W.M., Geballe T.R., 1989, A&A 222, 247.
Russell, A. P. G., Bally, J., Padman, R., Hills, R. E., 1992, ApJ 387, 219.
Schneider N., Csengeri T., Bontemps S. et al., 2010, arXiv1003.4198
Sternberg A., Dalgarno A., 1995, ApJS, 99, 565
van der Tak, F.F.S., Marseille M.G., Herpin F. et al. 2010 this volume
Wilson T.L., et al., 1995, ApJ 452, 693.

[1] LERMA, CNRS, Observatoire de Paris & Ecole Normale Supérieure, 24 rue Lhomond, 75005 Paris, France

[2] I. Physikalisches Institut der Universität zu Köln, Zülpicher Straße 77, 50937 Köln, Germany
[3] SRON Netherlands Institute for Space Research, P.O. Box 800, 9700 AV Groningen, Netherlands
[4] Institut d'Astrophysique Spatiale, CNRS and Université Paris-Sud, Bât. 121, 91405 Orsay Cedex, France
[5] Jet Propulsion Laboratory, Caltech, 4800 Oak Grove Drive, Pasadena CA 91109-8099, USA
[6] LERMA, CNRS & Observatoire de Paris , 61 av. de l'Observatoire, Paris, France
[7] CESR, CNRS and Université Paul Sabatier, 9 avenue du Colonel Roche, 31062 Toulouse, France
[8] Institute for Astronomy, ETH Zürich, 8093 Zürich, Switzerland
[9] Observatorio Astronómico Nacional (OAN), Apdo. 112, 28803 Alcalá de Henares (Madrid), Spain
[10] Max-Planck-Institut für Radioastronomie, Auf dem Hügel 69, 53121, Bonn, Germany
[11] Astronomy Department, University of Maryland, College Park, MD 20742, USA
[12] Instituto de Radio Astronomía Milimétrica (IRAM), Avenida Divina Pastora 7, Local 20, 18012 Granada, Spain
[13] IPAC/Caltech, MS 100-22, Pasadena, CA 91125, USA
[14] Department of Astronomy and Astrophysics, University of Toronto, 60 St. George Street, Toronto, ON M5S 3H8, Canada
[15] Centro de Astrobiología, CSIC-INTA, 28850, Madrid, Spain
[16] Department of Physics and Astronomy, John Hopkins University, 3400 North Charles Street, Baltimore, MD 21218, USA
[17] California Institute of Technology, 320-47, Pasadena, CA 91125-4700, USA
[18] Kapteyn Astronomical Institute, University of Groningen, PO box 800, 9700 AV Groningen, Netherlands
[19] European Space Astronomy Centre, Urb. Villafranca del Castillo, P.O. Box 50727, Madrid 28080, Spain
[20] University of Massachusetts, Astronomy Dept., Amherst, MA 01003-9305 U.S.A.
[21] Department of Physics and Astronomy, University of Waterloo, Canada N2L 3G1